Pulmonary Edema Monitoring Sensor with Integrated Body-Area Network for Remote Medical Sensing

Safa Salman, *Student Member, IEEE*, Zheyu Wang, *Student Member, IEEE*, Erin Colebeck, *Student Member, IEEE*, Asimina Kiourti, *Member, IEEE*, Erdem Topsakal, *Senior Member, IEEE*, and John L. Volakis, *Fellow, IEEE*.

Abstract—**A wearable health monitoring sensor integrated with a body-area network is presented for the diagnosis of pulmonary edema. This sensor is composed of 17 electrodes with 16 ports in-between and is intended to be placed on the human chest to detect lung irregularities by measuring the lung's average dielectric permittivity in a non-invasive way. Specifically, the sensor's active port is fed by a 40 MHz RF signal and its passive ports measure the corresponding amplitudes of the scattering parameters (S-parameters). The dielectric constant of the lung is then post-processed and expressed as a weighted sum of the S-parameters measured from each port. An important aspect of the sensor is the use of multiple electrodes which mitigates the effect of the outer layers (skin, fat and muscle) on the lung's permittivity. This allows for the characterization of deeper tissue layers. To validate the sensor, tissue-emulating gels were employed to mimic in-vivo tissues. Measurements of the lung's permittivity in both healthy and pulmonary edema states are carried out to validate the sensor's efficacy. Using the proposed post processing technique, the calculated permittivity of the lung from the measured S-parameters demonstrated error less than 11% compared to the direct measured value. Concurrently, a medical sensing body-area network (MS-BAN) is also employed to provide for remote data transfer. Measured results via the MS-BAN are well matched to those obtained by direct measurement. Thus, the MS-BAN enables the proposed sensor with continuous and robust remote sensing capability.**

Index terms **- Biomedical sensor, tissue dielectric properties, wearable sensor, medical sensing, body-area network, remote health monitoring.**

I. Introduction

PORTABLE and wearable medical sensors require continuous, unattended and uninterrupted monitoring of individual's health [1-6]. To meet this requirement, several sensors have been reported to provide accurate evaluation of the vital signals of the body. Already, a variety of commercial wearable sensors have been considered. Examples include: the VivoResponder [3], the WEALTHY wearable system [4] and others [5, 6]. Concurrently, diagnosis of severe diseases such as pulmonary edema requires deep tissue detection and monitoring. However, the aforementioned sensors lack this capability as they are limited to monitoring breathing, heart rate and skin temperature.

To address this issue, we present a wearable and non-invasive sensor for health monitoring. The proposed sensor is composed of 17 electrodes enabling monitoring of internal organs up to 10 cm deep into the torso [7]. We remark that the sensor works by gauging the fringing fields passing through the deep tissues and measuring the amplitude of the scattering parameters (S-parameters) at each port. These S-parameters are subsequently post processed to determine the tissue's permittivity. Importantly, the simplicity of the sensor design promotes real-time monitoring of internal organs in a care-free manner. This is advantageous for patients requiring supervised recovery from an acute event or surgical procedure. Such sensor is also beneficial for patients-at-risk and those with time sensitive diseases such as congestive heart failure or pulmonary edema.

In this paper, we first focus on the design and characterization of the proposed RF sensor towards the detection of early stages of pulmonary edema. Experimental validation of this RF sensor is then carried out on a human phantom integrated with a porcine lung to demonstrate its accuracy and feasibility in detecting irregularities of the lung. Concurrently, a body-area network for medical sensing (MS-BAN) is also developed and integrated with the sensor for continuous remote monitoring. Measurements of the RF sensor with MS-BAN are presented to demonstrate the robustness of the proposed remote medical sensing.

II. Sensor Structure and Development

The proposed sensor is composed of a finite set of electrodes as shown in Fig. 1(a). Port #1 is the active port and is excited by a monotonic RF signal at 40 MHz. The rest 15 passive ports are used for receiving the radiated fringing fields that propagated and dissipated through the tissues [7]. To characterize the underlying tissues, the amplitudes of the S-parameters between the sensor ports are measured. As shown in Fig. 1(b), these parameters are denoted as S_{i1}, where i = 2,

Manuscript received September 18th, 2013.
This work was supported in part by the National Science Foundation under grant 60033011 and the Office of Naval Research under grant 60029049.
S. Salman, Z. Wang, A. Kiourti, and J.L. Volakis are with the ElectroScience Laboratory, The Ohio State University, Columbus, OH 43212 USA. (e-mail: {salman.9, wang.1460, kiourti.1, volakis.1}@osu.edu).
Erin Colebeck and Erdem Topsakal are with Mississippi State University, Starkville, MS 39762 USA (e-mail: topsakal@ece.msstate.edu).

3, …, 16. We note that 50 Ω loads are placed across the unused ports to minimize undesirable reflections.

The unique features of the proposed sensor are the large penetration depth of the fields and the detection of small dielectric changes. These capabilities are owed to the sensor's large surface area and multiple signal probes across its surface. Concurrently, the sensor also provides suppression of unfavorable interference due to the outer human tissues (skin, fat, and muscle). That is, as shown in Fig. 1(b), the signals at the furthest (leftmost) electrodes are more dependent on the deep layer properties and vice versa. By exploiting this characteristic, we can suppress the interference of the outer human layers via post processing. This would provide for a more accurate determination of deep tissue permittivity (ε_r).

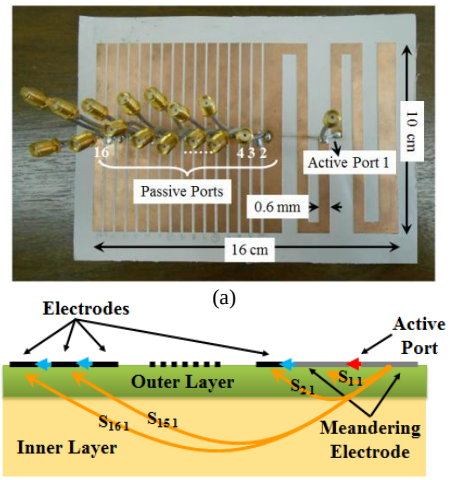

Fig. 1. (a) Fabricated sensor details, (b) side view of the fringing field penetration through the tissues where exploitation via post-processing allows for ε_r extraction for the inner layer.

I. Dielectric Constant Extraction from Scattering Parameters

Our main goal is to extract the average electrical properties of the tissue below the skin-fat-muscle layers. Thus, a multi-probe sensor of 16 cm in width and 10 cm in length will be utilized. The average permittivity is calculated for the inner layer volume where the fringing field of the electrode set is strongest. As mentioned in [7], that volume is estimated to be confined to the following dimensions: 16 cm in width x 10 cm in length x depth up to 10 cm (approximately 8 cm below the outer layers). To extract the dielectric constant, we propose to represent ε_r at this depth using a weighted sum of the measured amplitudes of the S-parameters (S_{i1}). Specifically, given that port #1 is active, ε_r can be expressed as

$$\varepsilon_r = \sum_{i=2}^{16} w_{i-1} S_{i1} \qquad (1)$$

In this, w_{i-1} represent the assigned weights (to be calculated) with i as the port number, and S_{i1} refer to the transmission coefficients measured across the passive ports. Weights w_{i-1} need to be carefully calculated in order to highlight ε_r changes in the deep inner layers while minimizing interference due to ε_r variations in the outer layers [7]. That is, (1) calibrates out the top layers. This is done by enforcing (1) while the deep tissue ε_r is kept constant and the outer layers (skin, fat, and muscle) in accordance to typical values of the human tissues [8, 9]. Variations in the outer layers were done by lumping the outer layers into one layer with average conductivity, permittivity and loss tangent. Then the properties of this layer are varied by a certain percentage [7]. For each variation, scattering parameters, S_{i1}, i = 2,.., N, were collected. Then this process was repeated for different inner tissue dielectrics and the S_{i1} data were collected again. The resulting equations (with S_{i1} and ε_r known and w_{i-1} as the unknowns) are then solved via the least square method to find the weights w_{i-1}. Simulations were done for phantoms using the human tissue emulating properties from [8, 9].

Following the above procedure, the trained equation (1) for extracting ε_r deep into the tissue depth was found to be:

$$\varepsilon_r = -2.85\,S_{21} - 0.82\,S_{31} + 5.22\,S_{41} + 2.91\,S_{51} - 0.19\,S_{61} + 0.69\,S_{71} + 4.95\,S_{81} + 4.06\,S_{91} + 7.22\,S_{10\,1} - 4.56\,S_{11\,1} + 4.22\,S_{12\,1} - 2.34\,S_{13\,1} - 6.51\,S_{14\,1} - 11.69\,S_{15\,1} - 2.00\,S_{16\,1} \qquad (2)$$

We remark that in the case of non-uniform tissues, the sensor is expected to extract the average permittivity value of tissue that lies underneath the sensor. For example, in the presence of a lung tumor ($\varepsilon_{tumor} \gg \varepsilon_{normal\ tissue}$ [10]), the average permittivity calculated by the sensor is expected to be larger than that of normal lung tissues. The case of a pulmonary edema will have a similar effect. This will be demonstrated in the study presented next.

II. Sample Study for Edema and Emphysema Symptoms

In order to test the robustness of the sensor along with the post processing technique, a simulation study of lung disease stages was carried out. Here we utilize the known volumetric percentages of tissue, air and blood to make a simulation representation of the lung in normal, edema and emphysema condition [11, 12]. Next the average ε_r of the lung is calculated for each condition as shown in Table I. Similarly, the average conductivity and loss tangent were calculated for the lung in each case. These values are assigned to the simulated inner layer (see Fig. 2) in three separate cases, with the outer layers (skin, fat and muscle) remaining the same. The S_{i1} data are collected at the passive ports and plugged into equation (2) to determine the permittivity.

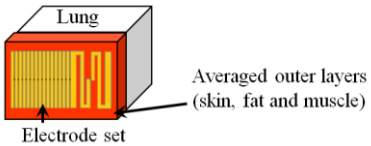

Fig. 2. Ansys® HFSS simulation model of the lung sensor with human tissue emulating layers.

TABLE I: Simulation Results and % Error

	Normal	Edema	Emphysema
Exact value of ε_r	34.20	51.20	16.90
Calculated ε_r using (2)	37.50	48.80	15.40
% Error	9.80	4.70	9.00

The calculated ε_r is shown in Table I along with the error rate compared to the exact values [8, 9]. As noted, the error remains below 10% for all cases.

With this simulation study, the sensor efficacy has been validated with low error rate. Next we proceed to experimental validation of the proposed sensor. Previous measurements were demonstrated in [7] using biological and non-biological material. However, we note that the electrical properties of the employed in-vitro biological material (e.g. ground beef and steak) depend on the temperature and freshness. Thus, they are not suitable to represent the real human body. In this paper we use tissue-emulating gels to better emulate human tissues. Details of the fabrication and RF characterization of these gels are demonstrated in the next section.

III. Tissue Emulation Technique

Various methods have been used in creating tissue emulating substances [13-16]. Particularly, solid phantoms [17-19] were used to measure the specific absorption rate (SAR). However, these tissue-emulating phantoms employed averaging of the electrical properties and thus did not represent the actual layered human tissue. To address this problem, we considered a multilayered phantom with each layer assigned individual tissue properties obtained from [20-24]. As shown in Fig. 3, a semi-solid gel based phantom was chosen because of its ease of fabrication and low cost.

As demonstrated in [25], the skin and muscle gels were created with a formula consisting of: Gelatin A, polyethylene glycol mono phenyl ether (Triton X-100), sodium chloride, de-ionizing water, vegetable oil, Ultra Ivory hand soap and food coloring. We note that the vegetable oil maintains the lowest electrical properties of the ingredients, whereas de-ionizing water has the highest. Concurrently, salt was added to increase conductivity and decrease the relative permittivity. By altering the mixture percentages, the properties of the tissue at 40 MHz can be emulated.

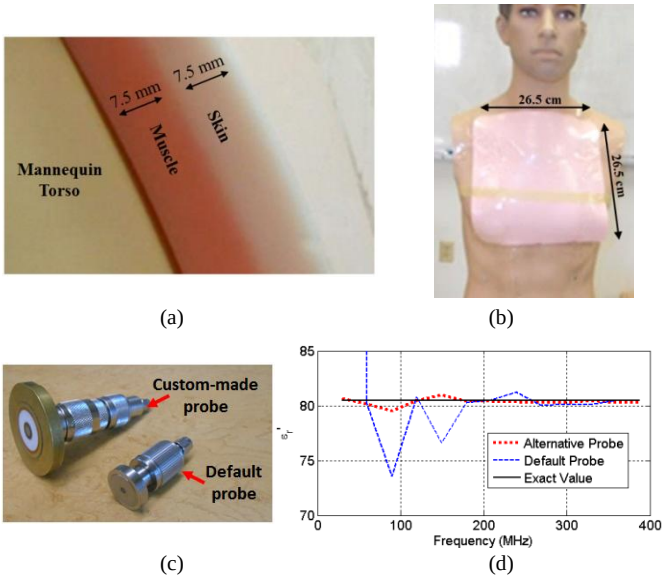

Fig. 3. (a) Cross-sectional view showing gel layers and thickness, (b) view of the mannequin with skin and muscle gel patches that mimic upper abdominal and chest, (c) default probe and the larger custom-made probe and (d) comparison of the performance of the probes in measuring distilled water.

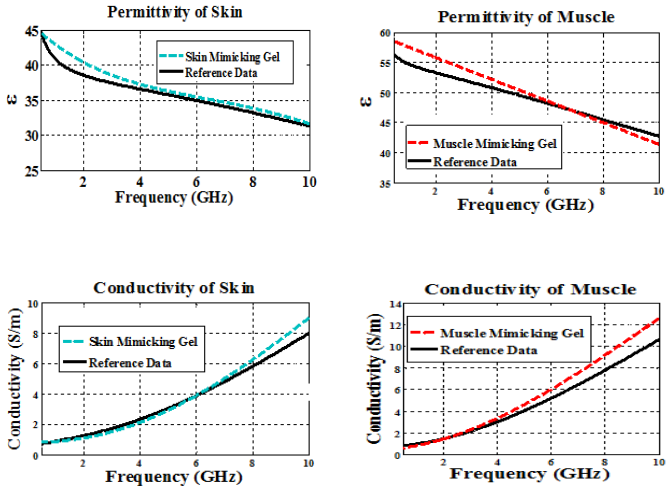

Fig. 4. Comparison between the exact electrical properties of human tissues [8] and the properties of fabricated gels for (a) skin, (b) muscle.

After the gel is cured completely, it is then placed at the mannequin's upper abdominal and chest region as seen in Fig. 3(b). To measure the RF characteristics of the gels, the Agilent® E8362B PNA Network Analyzer and Agilent® 85070E Dielectric Probe Kit were used. Because the default Agilent probe operates from 200 MHz to 20 GHz, a larger custom-made in-house open-ended coaxial probe is used for measurements below 200 MHz. The probe was designed using the open-ended coaxial technique [26] to extend the operation down in frequency (see Fig. 3 (c)). The custom-made probe works for dispersive material, such as distilled water, as shown in Fig. 3 (d).

As depicted in Fig. 4, measured results are demonstrated and compared to reference data from [8]. We remark that the measured properties of the tissue-emulating gels agreed well with the reference data, making it an appropriate representation of the phantom outer layers.

IV. Measurements Using a Human Phantom

We proceed to evaluate the sensor on a human phantom covered by the aforementioned tissue-emulating gels. Concurrently, a fresh porcine lung is also included inside the phantom (see Fig. 5(a)). We remark that the use of fresh porcine lung helps evaluate the sensor in a more realistic scenario, with unpredictable inhomogeneous characteristics introduced in the lung. The lung is secured in place using foam blocks and the lung sensor was placed on top of the multilayer gels as shown in Fig. 5(e). The phantom was then laid in the prone position and remains as such throughout the measurement to ensure that no air gaps existed between the lung and the phantom. We proceed to activate port #1 with a 40 MHz RF signal, and measure S_{i1} at the passive ports sequentially, with the rest unused ports terminated by 50 Ω. To ensure measurement accuracy, the data collection process was repeated twice, namely trial 1 and 2.

As shown in Fig. 5 (b), good match is found between the two trials of measurements. Concurrently, the exact ε_r of the porcine lung tissue was measured.

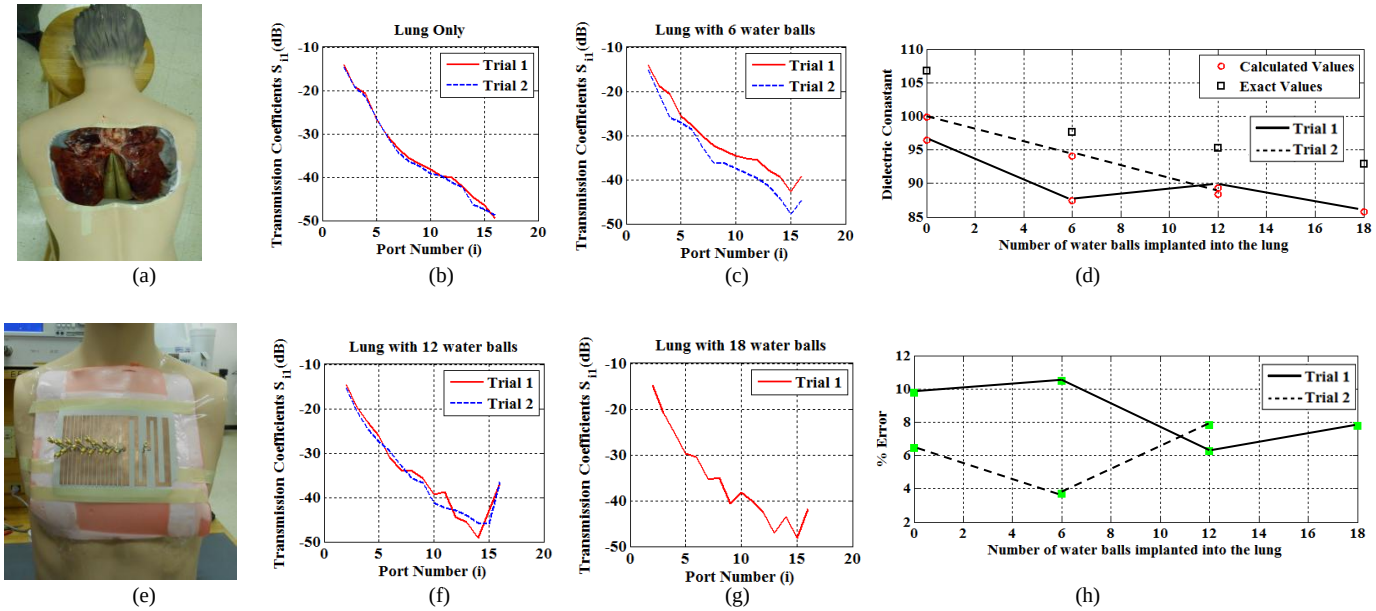

Fig. 5. (a) Porcine lung placement inside the mannequin torso, Transmission coefficients (S_{i1}) measured using the sensor (b) with porcine lung alone and(c) with 6 water balls inserted into the porcine lung, (d) Exact value vs. calculated value (using (2)) of the permittivity for different setups and different trials within each setup, (e) Gel layers and antenna placement on the outside of the mannequin torso, Transmission coefficients (S_{i1}) measured using the sensor (f) with 12 water balls inserted into the porcine lung and (g) with 18 water balls inserted into the porcine lung (h) Error rate for different setups and different trials within each setup.

TABLE II: CALCULATED VS. EXACT ε_r AND % ERROR

	Exact ε_r value	Calculated ε_r using (2)	% error
Lung Only Trial 1	106.80	96.4	9.74
Lung Only Trial 2	106.80	99.92	6.44
Six Water Balls Trial 1	97.67	87.47	10.44
Six Water Balls Trial 2	97.67	94.06	3.70
Twelve Water Balls Trial 1	95.30	89.37	6.22
Twelve Water Balls Trial 2	95.30	88.39	7.82
Eighteen Water Balls Trial 1	92.94	85.74	7.75

For reliability, the measurements were carried out multiple times and at different locations in the lung. The multiple measurements were then averaged to yield ε_r = 106.8 for the lung. Note that the lung tissue has a high ε_r in comparison to the values given in section IV due to being deflated and including embedded blood vessels.

As shown in Table II, differences between the calculated ε_r values using the sensor and the exact ε_r measured by dielectric probe are within 10%. These results are promising and demonstrate the feasibility of the RF sensor in detecting the dielectric permittivity of the lung.

Next, to simulate pulmonary edema stages, we proceeded to insert hollow plastic balls (diameter = 2 cm) filled with distilled water, inside the porcine lung. We started with 6 water balls placed randomly in the area where the sensor's fringing field is strongest. Following the previous measurement procedure, we obtained the S_{i1} data twice (see Fig. 5 (c)).

As shown in Table II, these results are compared to the exact ε_r which is calculated to be the volumetric proportion between lung tissue and distilled water, all within the area where the fringing field is strongest (16cm (L)×10cm (W)×8.5cm (H) below the gels). From Table II, we remark that error is maintained below 11%.

Note that at low frequencies [8, 9], the ε_r of lung tissue is higher than that of distilled water, thus the average ε_r of the lung + water is less than that of lung alone. Therefore, the dielectric constant of a water-filled lung may be lower than that of the deflated lung itself.

We proceed to increase the water balls incrementally by six. Measured results are shown in Fig. 5 (f, g) and in Table II. We found the errors between the calculated ε_r and the exact values are well below 11% (see Fig. 5(h)). We remark that, given the inhomogeneous characteristics of the lung tissue, low error rate is still achieved using the proposed RF sensor. This demonstrated the feasibility and robustness of the RF sensor. Additionally, we found all the calculate values of ε_r are smaller than the exact values measured by the dielectric probe at all times (see Fig. 5 (d, h)). To address this issue, a pre-measurement calibration is a likely option. Overall, the proposed RF sensor effectively determined the ε_r of the deep tissues, making it promising in detecting dielectric changes in the lung and monitoring the emergence of edema.

V. DESIGN OF THE BODY-AREA NETWORK FOR MEDICAL SENSING (MS-BAN)

A. *Architecture of the Body-Area Network*

To enable continuous remote sensing and data transfer, we proceed to develop a wireless body-area network [27] for medical sensing (MS-BAN). As shown in Fig. 6, we proposed a MS-BAN for the lung sensor. It was composed of the lung sensor and a compact body-area wireless communication system. To note, such wireless communication system was built by a wireless communication node and a Bluetooth bridge. To connect the RF sensor with the wireless communication system, a RF-to-DC converting circuit was also designed. As demonstrated in Fig. 6, the RF signal at the sensor output was first converted to DC signal and transferred

to the communication node. Then, it was transferred to the data collecting mobile devices via the Bluetooth bridge. We remarked that the collected data can be processed for in-situ display in a mobile application, and/or transferred to a cloud database for remote monitoring application.

Concurrently, reliable power supply was also critical in MS-BAN. In this study, we used battery for the proof of concept. A more sustainable solution is to employ energy harvesting aperture [28] on the body using wearable textile antennas [29, 30].

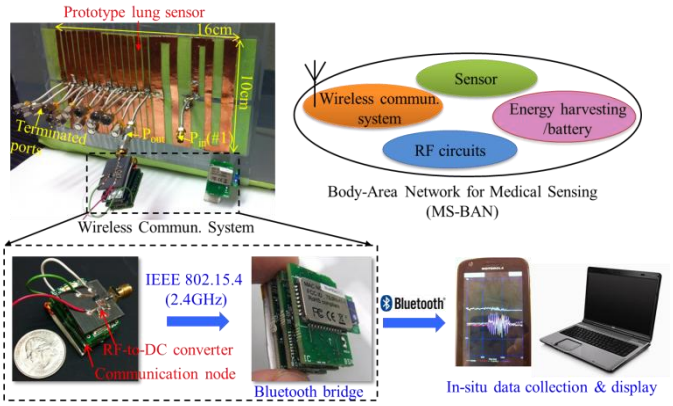

Fig. 6. Prototype lung monitoring sensor with integrated wireless communication system for MS-BAN.

1) Wireless communication system

As described in [27], the wireless communication system was composed of four basic functional boards: namely, a node board, an analog-to-digital conversion (ADC) board, a Bluetooth (BT) transmitter, and a rechargeable Li-Polymer battery board (see Fig. 7). The node board is compact in size (see Fig. 6), with a built-in microcontroller (TI MSP430) and a 2.4GHz IEEE 802.15.4 compliant RF transceiver (Chipcon CC2420). An embedded operating system (TinyOS [31]) was also included in the microcontroller for the wireless sensor network.

As demonstrated in [27], the input analog signal was first processed on the communication node and then transferred to the BT bridge via the RF transceiver, and eventually to the mobile device via a Bluetooth transmission. We noted that the communication range for the RF transceiver was ~5m, enough for the body-area network. Therefore, this compact wireless communication system provided a wireless data link for the development of MS-BAN.

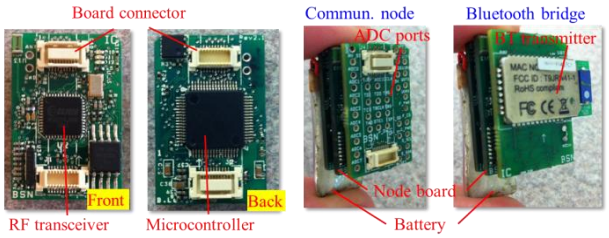

(a) (b)

Fig. 7. (a) Layout of the node board and (b) architectures of the communication node and Bluetooth bridge.

2) RF-to-DC converting circuit

The aforementioned wireless communication system required a DC input signal. Thus, a RF-to-DC signal conversion was critical to integrate the RF sensor with the wireless communication system. As shown in Fig 7 (a), a RF-to-DC converting circuit was designed and fabricated. It provided a broadband conversion of RF input signal from 100 kHz to 1GHz. We note that the key component of the converting circuit is the RF power detector chip (LTC5507 [32]). As described in [32], the RF input signal was peak detected by the Schottky diode peak detector inside the chip and supplied to the output pin. Multiple capacitors and resistors were also included for the proper function of the chip (see Fig. 8 (a)). Importantly, C_1 and C_2 were chosen based on the frequency range of the input RF signal [32]. That is, C_1 = C_2 = 0.1 μF for input signal ranged from 100 kHz to 30 MHz and C_1 = C_2 = 1000 pF for those from 30 MHz to 1GHz. Concurrently, C_3 = 100 pF and C_4 = 0.1 μF were used for power supply filters and R_1 = 400 Ω and R_2 = 12 Ω for input impedance matching.

As demonstrated in Fig. 8 (b), the output voltage of the converting circuit was measured. Two measurement methods were used, namely via a multimeter directly and via the wireless communication system. Notably, both measured results matched well, with error less than 7%. We remarked that this converting circuit provided a connection between the RF sensor and the wireless communication system with accuracy. Concurrently, as seen in Fig. 8 (b), we note that it was more accurate to detect V_{out} when RF_{in} > -17 dBm (steep region in the figure).

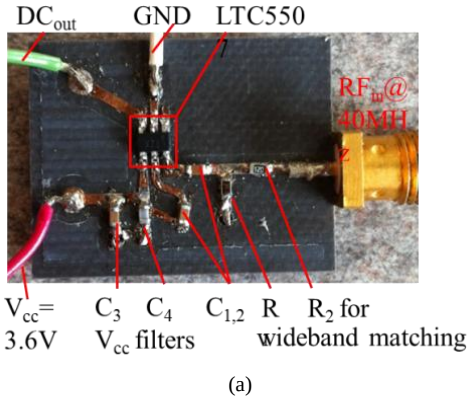

(a)

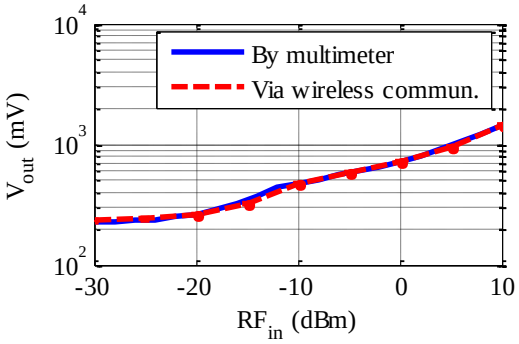

(b)

Fig. 8. (a) Fabricated RF-to-DC converting circuit and (b) measured DC output voltage with different RF input power at 40MHz.

B. *Experimental Validation of MS-BAN Wireless Link using Lung Sensor*

We then proceeded to integrate the aforementioned wireless communication system with the body-worn lung sensor to validate the MS-BAN wireless link. As shown in Fig. 9 (a), the lung sensor with the wireless system was mounted on the chest of the human phantom. Similar to the previous test, the chest was covered with skin and muscle layers made by tissue emulating gels and a fresh porcine lung was also placed inside the phantom. In this experiment, the wireless system was individually connected to each output port of the sensor with the rest terminated by 50 Ω loads. Then, the sensor input (port #1) was activated with 40 MHz RF signal. To ensure RF-to-DC converting accuracy, 15 dBm RF power was used at the sensor input. We note that the transmission coefficients S_{i1} were measured and transferred to a laptop via MS-BAN. As shown in Fig. 9 (b), the measured transmission coefficients of port #2 - 6 via MS-BAN was demonstrated. Notably, they are well matched with the measured result in the previous section (see Fig. 5 (b)). We remarked that MS-BAN wireless link enabled highly accurate data transmission in body-worn sensor application. This characteristic was very beneficial to remote medical monitoring.

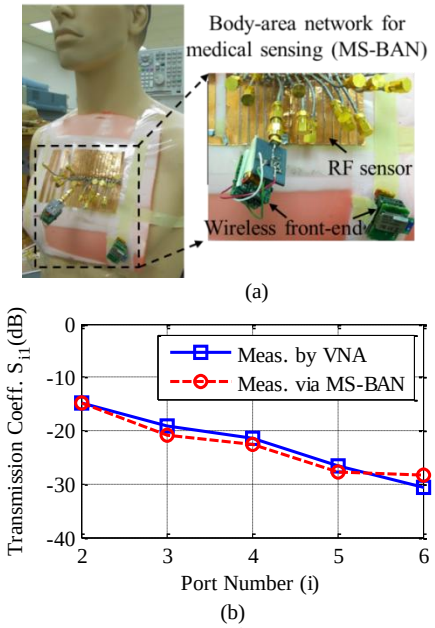

Fig. 9. (a) Experimental validation of MS-BAN wireless link using lung monitoring sensor and (b) comparison of measured transmission coefficient S_{x1} by VNA and via MS-BAN.

We note that the output power beyond port #6 of the sensor was too low to ensure RF-to-DC conversion accuracy. Better sensitivity is needed in the RF-to-DC converting circuit in order to improve the converting accuracy, i.e. better detection of input signals with low RF power. Thus, the use of a more sensitive RF power detector chip is required. The RF-to-DC circuit in [28] can detect an input power level as low as -40 dBm. By adapting this design, the sensitivity of the MS-BAN would increase, resulting in a more accurate wireless data transmission for all 16 ports. Concurrently, if only data from 6 ports were to be collected, the inner layer's permittivity could be measured to a depth of up to 4 cm because fringing field depth is proportional to the size of the sensor and the number of probes. In order to penetrate as deep as 10 cm, it is necessary to obtain data from all 16 ports. Further improvements and testing to the sensitivity of the RF-to-DC converting circuit will be done in the future.

VI. Concluding Remarks

The widespread advances in sensing and body-area networking technologies have led to a new paradigm for health care in the form of electronic heath monitoring systems. In this new paradigm, continuous time monitoring of the patient and data sensing and transfer are constantly demanded. In this paper, we provide a sensor that diagnoses the abnormalities of the deep tissues (especially the lung) through the identification of the average permittivity of the tissue. Moreover, we develop a body-area network (MS-BAN) to wirelessly transfer the data collected by the sensor for continuous health monitoring. We note that, given the inhomogeneity of the porcine lung tissue, the measured ε_r demonstrated error <11% at all time. The proposed sensor was also able to differentiate between stages of pulmonary edema. We note that error rate is expected to decrease significantly by employing calibration techniques (current under development). Further, testing of the MS-BAN technology was carried out with the sensor. Measured S-parameters using MS-BAN were in good agreement with the previous measured results. The experimental results validated the proposed body-area network for medical sensing and demonstrated its feasibility in the application of remote health monitoring.

References

[1] M. J. Kuhn, M. Awida, M. R. Mahfouz and A. E. Fathy, "Open-Ended Coaxial Probe Measurements for Breast Cancer Detection", *IEEE Radio and Wireless Symposium*, pp. 512-515, Jan 2010.

[2] M. E. Raabe and C. Davis, "Measuring Dielectric Properties of Simulants for Biological Tissue" Merit Fair 2011.

[3] A. Bonfiglio and D. De Rossi, Eds., *Wearable Monitoring Systems*, Springer, New York, NY, USA, 2011.

[4] R. Paradiso, G. Loriga, N. Taccini, "A Wearable Health Care System based on Knitted Integrated Sensors," *IEEE Transaction Technology in Biomedicine*, vol. 9 (3), pp.337-345, 2005.

[5] B. Liu, Y. Zhang and Z. Liu, "Wearable Monitoring System with Multiple Physiological Parameters" *Proceedings of the 5th International Workshop on Wearable and Implantable Body Sensor Networks, in conjunction with The 5th International Summer School and Symposium on Medical Devices and Biosensors*,pp. 268-271, June, 2008.

[6] A. Pantelopoulos and N. Bourbakis, "A formal language approach for multi-sensor wearable health-monitoring systems," *IEEE International BioInformatics and BioEngineering Conference, 2008.*

[7] S. Salman, D. Psychoudakis, J. L. Volakis, "Determining the Relative Permittivity of Deep Embedded Biological Tissues," *IEEE Antenna and Propagation Letters*, vol. 11, pp. 1694-1697, 2012.

[8] S. Gabriel, R. W. Lau and C. Gabriel, "The dielectric properties of biological tissues—Part II: Measurement in the frequency range 10 Hz to 20 GHz," *Physics in Medicine and Biology*, vol. 41, pp. 2251–2269, 1996.

[9] C. Gabriel, "Compilation of the dielectric properties of body tissues at RF and microwave frequencies," Report N.AL/OE-TR- 1996-0037, Occupational and environmental health directorate, Radiofrequency Radiation Division, Brooks Air Force Base, Texas (USA), June 1996.

[10] M. Lazebnik, D. Popovic, L. McCartney, C. B. Watkins, M. J. Lindstrom, J. Harter, S. Sewall, T. Ogilvie, A. Magliocco, T. M. Breslin, W. Temple, D. Mew, J. H. Booske, M. Okoniewski and S. C. Hagness,

"A large-scale study of the ultrawideband microwave dielectric properties of normal, benign and malignant breast tissues obtained from cancer surgeries," *Physics in Medicine and Biology*, vol. 52, pp. 6093-6115, 2007.

[11] P.C. Pedersen, C.C. Johnson, C.H. Durney, D.C. Bragg, "Microwave reflection and transmission measurements for pulmonary diagnosis and monitoring", *IEEE Transaction on Biomedical Engineering*, vol. 25, pp. 40–48, 1978.

[12] S. Watanabe, M. Mitchell, A. D. Renxetti, "Correlation of structure and function in chronic pulmonary emphysema," *The American Review of Respiratory Disease*, vol. 92, pp. 221–227, 1965.

[13] M. Ballen, M. Kanda, C. K. Chou, and Q. Balzano, "Formulation and characterization of tissue simulating liquids used for SAR measurement," *Proc. 23rd Annual Bioelectromagnetics Society. Meeting*, vol. 14 (3), pp. 80, 2001.

[14] K. Fukunaga, S. Watanabe, and Y. Yamanaka, "Dielectric properties of tissue equivalent liquids and their effects on specific absorption rate," *IEEE Transaction on Electromagnetic Compatibility*, vol. 46 (1), pp. 126–129, 2004.

[15] K. Fukunaga, S. Watanabe, H. Asou and K. Sato, "Dielectric properties of non-toxic tissue-equivalent liquids for radiowave safety tests," *IEEE International Conference on Dielectric Liquids*, pp. 425-428, 2005.

[16] J. Kim and Y. Rahmat-Samii, "Implanted antennas inside a human body: Simulations, designs, and characterizations," *EEE Transaction on Microwave Theory and Techniques*, vol. 52 (8), pp. 1934–1943, 2004.

[17] Y. Nikawa, M. Chino, and K. Kikuchi, "Soft and dry phantom modeling material using silicone rubber with carbon fiber," *IEEE Transaction on Microwave Theory and Techniques*, vol. 44, pp. 1949–53, 1996.

[18] C. Gabriel, "Tissue equivalent material for hand phantoms," *Physics in Medicine and Biology*, vol. 52, pp. 4205-4210, 2007.

[19] S. Stuchly, "Specific absorption rate distributions in a heterogeneous model of the human body at radio frequencies," *Environmental Protection Agency Project Summary*, pp. 89, 1987.

[20] A. Surowiec, P. N. Shrivastava, M. Astrahan, and Z. Petrovich, "Utilization of a multilayer polyacrylamide phantom for evaluation of hyperthermia applicators," *International Journal of Hyperthermia*, vol. 8, pp. 795–807, 1992.

[21] C. K. Chou, G. W. Chen, A. W. Guy, and K. H. Luk, "Formulas for preparing phantom muscle tissue at various radiofrequencies," *Bioelectromagnetics*, vol. 5, pp. 435–41, 1984.

[22] K. Ito, K. Furuya, Y. Okano, and L. Hamada, "Development and characteristics of a biological tissue-equivalent phantom for microwaves," *Electronics and Communications in Japan Part I*, vol. 84, pp. 1126–35, 2001.

[23] T. Sunaga, H. Ikehira, S. Furukawa, M. Tamura, E. Yoshitome, T. Obata, H. Shinkai, S. Tanada, M. Hajime, and Y. Sasaki, "Development of a dielectric equivalent gel for better impedance matching for human skin," *Bioelectromagnetics*, vol. 24, pp. 214–17, 2003.

[24] D. Miklavčič, N. Pavšelj, and F. X. Hart, "Electric properties of tissues," *Wiley Encyclopedia of Biomedical Engineering*, John Wiley & Sons, pp. 1-12, 2006.

[25] T Yilmaz, T Karacolak, and E Topsakal, "Characterization and testing of a skin mimicking material for implantable antennas operating at ISM band (2.4 GHz-2.48 GHz)," Antennas and Wireless Propagation Letters, IEEE 7, 418-420.

[26] W. Ellison, and J.-M. Moreau, "Open-ended coaxial probe: Model limitations," *IEEE Transactions on Instrumentation and Measurement*, vol. 57(9), pp. 1984-1991, 2008.

[27] G. Yang, Ed., *Body Sensor Networks*, Springer, London, UK, 2006.

[28] U. Olgun, C.-C. Chen, J.L. Volakis, "Design of an efficient ambient WiFi energy harvesting system," *IET Microwaves, Antennas & Propagation*, vol.6 (11), pp.1200-1206, 2012.

[29] Z. Wang, L. Zhang, Y. Bayram, and J. L. Volakis, "Embroidered conductive fibers on polymer composite for conformal antennas," *IEEE Transaction on Antennas Propagation*, vol. 60 (9), pp. 4141–4147, 2012.

[30] Z. Wang, L.Z. Lee, D. Psychoudakis, and J. L. Volakis, "Embroidered multiband body-worn antenna for GSM/PCS/WLAN communications," submitted to *IEEE Transactions on Antennas Propagation*, 2013.

[31] J.L. Hill, "System architecture for wireless sensor networks," University of California Berkeley, PhD Thesis, 2003.

[32] LTC5507 100 kHz to 1GHz RF Power Detector, Linear Technology, [online]. Available: http://www.linear.com/product/LTC5507.

Safa Salman was born in Baghdad, Iraq, in 1989. She received the B.S. degree (summa cum laude) from the University of Mississippi, Oxford, Mississippi, in 2010 with an honors degree from the Sally McDonnell Barksdale Honors College, Oxford, Mississippi. She also received the Taylor medal for her distinguished academic achievements.

She is currently pursuing her Doctoral degree at the ElectroScience Laboratory, The Ohio State University. Her research areas include Broadband arrays, biomedical applications of antennas, implanted antennas, ablation techniques and wearable continuous time health monitoring sensors.

Ms. Salman placed at first place in the annual Kraus memorial student poster competition, received the ARO student paper competition scholarship at the 11th international workshop on finite elements for microwave engineering, nominated for the 2010 Exxon Mobile Middle East & South Africa Scholarship and selected for the 2009-2010 Who's Who among students in American Universities and Colleges. She is a member of honor societies such as Phi Kappa Phi, Tau Beta Pi, Eta Kappa Nu and the National Society of Collegiate Scholars.

Zheyu Wang (S'10) received his B.S. degree in electrical engineering from University of Electronic Science and Technology of China, Chengdu, China, in 2009. He is currently pursuing the Ph.D. degree at the Ohio State University, Columbus, Ohio.

He has been a Graduate Research Associate at OSU ElectroScience Laboratory since 2009, where he conducts research on body-worn antennas and wearable radio frequency electronics, novel materials and structures for body-worn applications, and radio frequency energy harvesting. His research has been reported on *BBC News* and *Discovery News*.

Mr. Wang received the IEEE AP-S Doctoral Research Award in 2013, the Best Paper Award at 2012 IEEE IWAT conference, the National Radio Science Fellowship Award from URSI in 2012, and the Best Undergraduate Thesis Award from UESTC in 2009.

Asimina Kiourti (S'10, M'14) received the Diploma in Electrical and Computer Engineering from the University of Patras, Greece (2008), the MSc in Technologies for Broadband Communications from University College London, U.K. (2009), and the PhD degree in Electrical and Computer Engineering from the National Technical University of Athens, Greece (2013).

Dr. Kiourti is currently a Postdoctoral Researcher at the ElectroScience Laboratory of The Ohio State University. She has authored or co-authored more than 40 journal and

conference papers and 4 book chapters. Her research interests include antennas for medical applications, medical sensing, RF circuits, bioelectromagnetics, and flexible textile and polymer-based antennas.

Dr. Kiourti has received various awards and scholarships, among which, the IEEE MTT-S Graduate Fellowship for Medical Applications for 2012 and the IEEE AP-S Doctoral Research Award for 2011. She is a member of the Technical Chamber of Greece and the IEEE.

Erdem Topsakal received his BSc., M.Sc., and PhD degrees in 1991, 1993, and 1996 in Electronics and Communication Engineering from Istanbul Technical University. He was a post-doctoral fellow from 1998 to 2000 and an assistant research scientist from 2000 to July 2003 in Electrical Engineering and Computer Science Department of the University of Michigan, Ann Arbor. In August 2003, he joined the Electrical and Computer Engineering Department of James Worth Bagley College of Engineering at Mississippi State University as an Assistant Professor. He is currently a tenured Associate Professor in the same department. His research areas include wireless medical telemetry, implantable antennas, cancer monitoring and detection, microwave hyperthermia, fast electromagnetic methods, antenna analysis and design, direct and inverse scattering. He has published over 150 journal and conference papers in these areas. He received the URSI young scientist award in 1996 and NATO fellowship in 1997. He is the recipient of 2004-2005 Mississippi State University Electrical and Computer Engineering Department outstanding educator award, 2009 Bagley College of Engineering Research Paper of the Year Award, and 2011 and 2012 Mississippi State University State Pride Award. In addition, he has over 20 national/international awards with his undergraduate and graduate students. He is a senior member of IEEE and an elected member of the URSI commissions B and K. He currently serves as the Associate Editor for IEEE Antennas and Wireless Propagation Letters (AWPL), Associate Editor for URSI Radio Science Bulletin, and Chair for URSI United States National Committee Commission K, Electromagnetics in Biology and Medicine. He is the upcoming Chair for the student paper competition for URSI-USNC. He is on the IEEE USA Committee on Communications& Information Policy as a representative of IEEE Engineering in Medicine and Biology Society. He is a member of National Institute of Health SBIB (10) Biomedical Imaging study section and a member of IEEE Microwave Theory and Techniques Society Technical Committee MTT-10, Biological Effect and Medical Applications of RF and Microwaves. In addition, he routinely reviews proposals for NIH, NSF and DoD. He is a member of electrical engineering honor society, eta kappa nu. He is the founder and has been the dance instructor of Mississippi State University Ballroom Dance club since 2005.

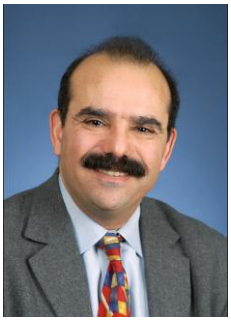

John L. Volakis (S'77-M'82-SM'89-F96) was born on May 13, 1956 in Chios, Greece and immigrated to the U.S.A. in 1973. He obtained his B.E. Degree, summa cum laude, in 1978 from Youngstown State Univ., Youngstown, Ohio, the M.Sc. in 1979 from The Ohio State Univ., Columbus, Ohio and the Ph.D. degree in 1982, also from the Ohio State Univ.

Prof. Volakis started his career at Rockwell International (1982-84), now Boeing. In 1984, he was appointed Assistant Professor at The University of Michigan, Ann Arbor, MI, becoming a full Professor in 1994. He also served as the Director of the Radiation Laboratory from 1998 to 2000. Since January 2003, he is the Roy and Lois Chope Chair Professor of Engineering at the Ohio State University, Columbus, Ohio and also serves as the Director of the ElectroScience Laboratory. Over the years, he carried out research in antennas, wireless communications and propagation, computational methods, electromagnetic compatibility and interference, design optimization, RF materials, multi-physics engineering, millimeter waves, terahertz and medical sensing. His publications include 8 books, 340 journal papers, nearly 600 conference papers and 23 book chapters. Among his co-authored books are: *Approximate Boundary Conditions in Electromagnetics*, 1995; *Finite Element Methods for Electromagnetics*, 1998; 4th *edition Antenna Engineering Handbook*, 2007; *Small Antennas*, 2010; and *Integral Equation Methods for Electromagnetic*s, 2011). He has graduated/mentored over 75 doctoral students/post-docs with 20 of them receiving best paper awards at conferences. His service to Professional Societies include: 2004 President of the IEEE Antennas and Propagation Society (2004), Vice Chair of USNC/URSI Commission B, twice the general Chair of the IEEE Antennas and Propagation Symposium, IEEE APS Distinguished Lecturer, IEEE APS Fellows Committee Chair, IEEE-wide Fellows committee member & Associate Editor of several journals. He is listed by ISI among the top 250 most referenced authors (2004), and is a Fellow of IEEE and ACES. Among his awards are: The Univ. of Michigan College of Engineering Research Excellence award (1993), Scott award from The Ohio State Univ. College of Engineering for Outstanding Academic Achievement (2011) and the IEEE AP Society C-T. Tai Teaching Excellence award (2011).